Proceedings of CONF-MSS 2026 Symposium: Advanced Composite Materials and Polymer Chemistry
DOI: 10.54254/2755-2721/2026.AD33327

Research Progress in Cathode Materials for Lithium-Ion Batteries

Zhonghan Lin

School of Materials Science and Engineering, Ocean University of China, Qingdao, China
2035462279@qq.com

Abstract. Since the commercialization of lithiumion batteries in the 1990s, they have been extensively applied in portable electronics, electric vehicles, and energystorage systemsowing to their high energy density, long cycle life, low selfdischarge rate, and environmental benignity. As the core component determining the capacity and stability of lithiumion batteries, cathode materials play a decisive role in overall electrochemical performance. This paper briefly reviews the developmental history, fundamental structure, and operating mechanism of lithiumion batteries, then focuses on three major categories of commercial and researchoriented cathode materials: olivinetype lithium iron phosphate ($LiFePO_4$), spinelstructured lithium manganese oxide ($LiMn_2O_4$) and its highvoltage derivatives such as $LiNi_{0.5}Mn_{1.5}O_4$, as well as layered oxide systems including $LiCoO_2$, $LiNiO_2$, NiCoMn (NCM) ternary materials, and lithiumrich manganesebased layered oxides. It systematically compares their crystal structures, electrochemical characteristics, inherent drawbacks, and common modification strategies, with the purpose of offering theoretical support and technical guidance for the rational design and industrial application of advanced cathode materials.

Keywords: Lithium-ion batteries, Cathode materials, Modification

1. Introduction

With the continuous development of electrolytes matching metallic lithium anodes, in the early 1970s, primary lithium batteries were commercialized using metallic Li as the anode and MnO_2 or $SOCl_2$ as the cathode, and attention was turned to rechargeable secondary lithium batteries. On the basis of primary lithium batteries, novel cathode materials capable of reversible lithium ion intercalation/deintercalation were developed, promoting the advancement of rechargeable batteries (known as secondary batteries). In 1972, Professor Whittingham from Exxon reported a new cathode material—TiS_2, and fabricated the world's first rechargeable secondary lithium battery [1-3]. In TiS_2, Li^+ can repeatedly intercalate and deintercalate between layers of transition metal sulfides. In this study, Professor Whittingham first proposed the battery working principle based on intercalation reactions, laying the foundation for the development of lithium-ion secondary batteries. In 1991, Sony Corporation launched the world's first commercial lithium-ion battery using lithium cobalt oxide as the cathode and petroleum coke as the anode material. Upon its launch, lithium-ion batteries quickly occupied the energy market and promoted the miniaturization and thinning of

DOI: 10.54254/2755-2721/2026.AD33327

electronic products due to their advantages of high voltage [4], small size [5], high energy density and green pollution-free characteristics. In the future, with the continuous innovation of portable electronic products and the rapid development of new energy vehicles, the lithium-ion battery market will further expand and become an indispensable part of society.

The cathode is one of the indispensable components of lithium-ion batteries, accounting for about 40% of the battery production cost and 43% of the mass in common commercial pouch batteries. Therefore, cathode materials exert a crucial impact on the comprehensive performance of the entire battery. Ideal cathode materials for lithium-ion batteries should possess the following characteristics: the compound $Li_xM_\gamma Xz$ can undergo extensive reversible Li^+ intercalation/deintercalation, which requires the material to have sufficient redox couples and lithium storage sites to provide a high specific capacity. The transition metal ion M has a high redox potential to increase the output voltage of the battery. The compound needs a stable structural framework to avoid structural decay during Li^+ intercalation/deintercalation throughout the charge-discharge process, ensuring the cycle stability of the battery. The redox potential should change as little as possible with the variation of x to provide a stable working voltage plateau during battery operation. The compound has good electronic conductivity and Li^+ migration rate to achieve rapid electron and ion conduction under high-rate charge-discharge. The compound also requires certain chemical and thermal stability to meet the safety requirements of practical battery applications. The synthetic raw materials of the material should select elements with abundant natural resources, low cost and environmental friendliness, and simple synthetic methods should be adopted as much as possible to reduce the production cost of cathode materials.

At present, the research and development of cathode materials for lithium-ion batteries mainly focus on three directions: olivine-structured polyanion materials (e.g., $LiFePO_4$), spinel-phase lithium manganese oxide materials (e.g., $LiMn_2O_4$), and layered-phase metal oxide materials (e.g., $LiCoO_2$). This paper mainly summarizes olivine, spinel and layered materials.

2. Preparing your paper

2.1. Basic structure

Between 1996 and 1997, NNT Corporation of Japan and Professor Goodenough of the University of Texas at Austin successively reported the characteristics of olivine-phase structure $A_\gamma MPO_4$ (A is alkali metal, M is a combination of Co and Fe) and its typical representative lithium iron phosphate $LiFePO_4$ as a cathode material for reversible Li^+ intercalation/deintercalation. The crystal structure of $LiFePO_4$ is shown in Figure 1, belonging to the Pnma space group. In this crystal structure, O is arranged in a slightly distorted hexagonal close-packed manner, Li^+ and Fe^{2+} occupy the 4a and 4c octahedral sites of the structure respectively, and P occupies the 4c tetrahedral site. In the structure, FeO_6 octahedra are connected to four surrounding FeO_6 octahedra in a corner-sharing manner, forming a zigzag planar layer; PO_4 tetrahedra are connected to FeO_6 octahedra in a corner-sharing or edge-sharing manner, and the spatial framework composed of PO_4 and FeO_6 forms a one-dimensional lithium ion transport channel along the [010] direction. The practical specific capacity of $LiFePO_4$ is generally 150 mAh g^{-1} (the theoretical specific capacity is 170 mAh g^{-1}), and its charge-discharge curve shows a long plateau at 3.4 V (vs Li/Li^+), which is generally considered to correspond to the two-phase reaction between $LiFePO_4$ and $FePO_4$. Since $FePO_4$ and $LiFePO_4$ have similar crystal structures and close unit cell parameters, the unit cell volume change during charge-discharge is only about 6.5%, maintaining the crystal phase structure stability during charge-discharge, thus exhibiting good cycle stability.

DOI: 10.54254/2755-2721/2026.AD33327

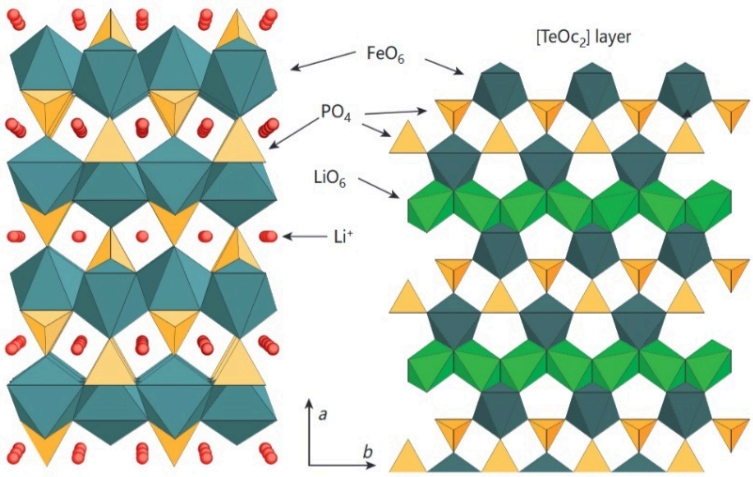

Figure 1. Schematic diagram of the $LiFePO_4$ structure

$LiFePO_4$ has low intrinsic electronic/ionic conductivity and is not suitable for high-rate charge-discharge. On the one hand, the FeO_6 octahedra in the crystal structure are connected by corner-sharing, restricting electron transport along the O-Fe-O channel, so $LiFePO_4$ has an electronic conductivity of only 10^{-9} S cm^{-1}. On the other hand, the hexagonal close-packed oxygen ion framework and dispersed PO_4 polyanions hinder the migration of Li^+ in the framework structure. Therefore, $LiFePO_4$ was considered unable to meet commercial use in the early stage and did not attract widespread attention. However, with continuous exploration and improvement by researchers, a series of effective improvement measures have been discovered to enhance the electronic conductivity of $LiFePO_4$ and the transport rate of ions in the crystal: (1) Regulating the morphology and size of the material, such as synthesizing porous materials or nanoparticles with high specific surface area to shorten the Li^+ transport path and improve Li^+ transport efficiency. (2) Conducting surface conductive layer coating, the most common being carbon coating on the surface of $LiFePO_4$ to increase electronic conductivity and improve electrochemical performance. (3) Cationic doping of $LiFePO_4$ to replace part of Li^+ and Fe^{2+} can suppress lattice shrinkage and improve the intrinsic conductivity of the material. After these improvements, the high-rate charge-discharge performance of $LiFePO_4$ has been optimized. Meanwhile, due to its advantages of abundant raw material sources, low cost, environmental friendliness and stable cycle, $LiFePO_4$ is highly favored by the market and occupies a considerable market share in the power battery field.

2.2. Research progress of olivine-structured $LiMPO_4$ cathode materials: synthesis, modification and electrochemical performance

Olivine-structured phosphate cathode materials $LiMPO_4$ (M = Fe, Mn, Co, Ni) all belong to the orthorhombic system (Pnma space group) with the same basic structural framework, and the difference mainly lies in the type of transition metal ions occupying the octahedral (4c) sites. Different redox couples of M ions (e.g., Fe^{2+}/Fe^{3+}, Mn^{2+}/Mn^{3+}, Co^{2+}/Co^{3+}, Ni^{2+}/Ni^{3+}) determine their different working voltage plateaus, bringing different energy density advantages and practical application challenges. $LiFePO_4$ has been commercialized on a large scale due to its excellent cycle stability, safety and cost advantages, while the research on other members ($LiMnPO_4$, $LiCoPO_4$, $LiNiPO_4$) and their solid solutions (e.g., $LiFe_xMn_{1-x}PO_4$) is dedicated to overcoming their inherent defects to further improve energy density or explore high-voltage systems.

DOI: 10.54254/2755-2721/2026.AD33327

2.2.1. $LiNiPO_4$

$LiNiPO_4$ has an extremely high redox potential (~5.1 V vs. Li^+/Li), making its theoretical energy density very attractive, but it also poses a severe challenge to the electrochemical stability window of electrolytes. In addition, its inherent electronic/ionic conductivity is extremely low, and Li/Ni cation mixing is prone to occur during synthesis, leading to difficulty in exerting electrochemical activity. Padhi et al. first synthesized $LiNiPO_4$ via high-temperature solid-state method in their pioneering research, but the obtained material showed almost no electrochemical activity in conventional electrolytes. Subsequent studies mostly focused on nanocrystallization and surface modification to improve its performance. For example, Wang et al. successfully prepared carbon-coated nanoparticles via sol-gel method combined with subsequent annealing treatment. The introduction of the carbon layer constructed a continuous electronic conductive network on the particle surface, effectively improving the interfacial charge transfer kinetics. By adjusting the ratio of precursor to carbon source, they obtained samples with a particle size of about 50 nm, whose initial discharge specific capacity reached about 120 mAh g^{-1} at an extremely high cut-off voltage (>5.0 V). Electrochemical impedance spectroscopy (EIS) tests showed that the charge transfer resistance (Rct) of the optimized material was reduced by an order of magnitude compared with the uncoated sample, which was directly attributed to the improvement of electrode/electrolyte interface stability and the shortening of electron transport paths by carbon coating.

2.2.2. $LiCoPO_4$

$LiCoPO_4$ has a working voltage plateau of about 4.8 V, also facing the problem of high-voltage electrolyte compatibility. Its theoretical specific capacity is 167 mAh g^{-1}. Bramnik et al. systematically studied the effects of different synthesis methods on the structure and performance of $LiCoPO_4$. They compared solid-state method, hydrothermal method and sol-gel method, and found that precursors with uniform chemical composition and fine primary particle size (about 100-200 nm) could be prepared via sol-gel method combined with specific chelating agents (e.g., citric acid), and pure-phase materials with good crystallinity were obtained after subsequent annealing. To further improve conductivity, Martha et al. introduced reduced graphene oxide (rGO) during the sol-gel process, forming a composite structure in which $LiCoPO_4$ nanoparticles were anchored on the three-dimensional conductive network of rGO. This structure not only greatly improved the overall electronic conductivity, but also its abundant pore structure was conducive to electrolyte infiltration and rapid lithium ion transport. The prepared composite exhibited a capacity close to the theoretical value (~165 mAh g^{-1}) at 0.1C rate, and the rate performance was significantly improved. EIS tests confirmed that the Rct value of this composite was reduced by about 70% compared with the sample prepared by traditional solid-state method, mainly due to the fast electron channels and stable interface structure provided by the rGO network.

2.2.3. $LiMnPO_4$

$LiMnPO_4$ has a higher voltage plateau (~4.1 V) than $LiFePO_4$ (~3.45 V), thus having higher energy density potential, but its electronic conductivity and ion diffusion coefficient are even lower than those of $LiFePO_4$, and the Jahn-Teller effect of Mn^{3+} during charge-discharge easily leads to structural distortion and capacity fading. Oh et al. successfully synthesized $LiMnPO_4$ with specific morphologies (e.g., nanosheets, nanorods) via polyol-mediated solvothermal method by precisely controlling the reaction temperature and the concentration of surfactant (e.g., oleylamine). They

DOI: 10.54254/2755-2721/2026.AD33327

further formed an amorphous carbon layer with a thickness of about 2-3 nm on the particle surface through in-situ carbon coating. This uniform carbon layer significantly enhanced the electronic contact between particles and increased the electronic conductivity of the material by several orders of magnitude. The optimized $LiMnPO_4$/C material could deliver a high specific capacity of up to 168 mAh g^{-1} at 0.05C rate, close to its theoretical value (171 mAh g^{-1}). In addition, Kwon et al. reported the preparation of micron-scale secondary spherical $LiMnPO_4$/C composites via ionic liquid-assisted ball milling combined with spray drying technology, whose secondary spheres were composed of numerous nano primary particles. This "micro-nano" hierarchical structure effectively shortened the solid-state diffusion path of lithium ions while ensuring high tap density. The material had a capacity retention rate of more than 90% after 200 cycles at 1C rate. EIS analysis showed that the Rct growth of the optimized sample after cycling was much smaller than that of the unoptimized sample, proving its superior structural and interface stability.

2.2.4. $LiFe_xMn_{1-x}PO_4$ solid solution

To balance high voltage (contributed by Mn) and high conductivity/stability (contributed by Fe), $LiFe_xMn_{1-x}PO_4$ solid solution has become a research hotspot. However, the different kinetic behaviors of Fe and Mn during charge-discharge and the Jahn-Teller effect of Mn^{3+} make its cycle stability face challenges, especially when the Mn content is high (x is small). Yamada et al. first reported that $LiFe_{0.5}Mn_{0.5}PO_4$ solid solution nanocrystals with uniform composition could be prepared via coprecipitation method combined with hydrothermal reaction. Wang et al. developed a carbothermal reduction method based on iron/manganese phosphate precursors, realizing simultaneous crystallization and carbon coating of the material through one-step high-temperature sintering. They systematically studied the effect of Fe/Mn ratio on electrochemical performance and found that when x=0.6-0.8, the material could achieve a good balance between energy density and cycle life. To further improve the performance of high-Mn content solid solutions, Shin et al. synthesized Mg^{2+} gradient-doped $LiFe_{0.3}Mn_{0.7}PO_4$/C materials via sol-gel method. They regulated the concentration distribution of Mg^{2+} during synthesis to make it enriched on the particle surface. This surface doping strategy effectively inhibited the severe Jahn-Teller distortion and electrolyte side reactions induced by Mn^{3+} on the particle surface, thus stabilizing the interface. The prepared material had a discharge specific capacity of 155 mAh g^{-1} at 0.2C rate and a capacity retention rate of up to 95% after 500 cycles at 1C rate. EIS analysis of electrodes at different cycle stages confirmed that the Rct increase of the gradient Mg-doped sample with cycling was much smaller than that of undoped or bulk uniformly doped samples, highlighting the key role of surface engineering in stabilizing the electrochemical interface of solid solution materials.

3. Spinel-phase cathode materials

In 1983, Goodenough's research group first reported the reversible Li^+ intercalation/ deintercalation ability of spinel-structured $LiMn_2O_4$. The crystal structure of $LiMn_2O_4$ is shown in Figure 2a, belonging to the cubic system with the Fd-3m space group. Each unit cell contains 32 O atoms arranged in face-centered cubic close packing (FCC), occupying the 32e site. Li^+ and $Mn^{3+/4+}$ occupy the tetrahedral 8a site and octahedral 16d site in the cubic close-packed oxygen distribution respectively. In the framework structure, MnO_6 octahedra are connected to each other in an edge-sharing manner, forming a stable Mn_2O_4 skeleton. Since Li^+ and $Mn^{3+/4+}$ only occupy 1/4 of the corresponding sites, there are a large number of vacancies in the spinel structure (Figure 2b). The LiO_4 tetrahedra at the 8a site are connected to the vacant oxygen octahedra at the 16c site in a face-

DOI: 10.54254/2755-2721/2026.AD33327

sharing manner, forming a three-dimensional ion diffusion channel—Li^+ can migrate along the 8a→16c→8a path in the structure. Therefore, $LiMn_2O_4$ has excellent Li^+ migration ability.

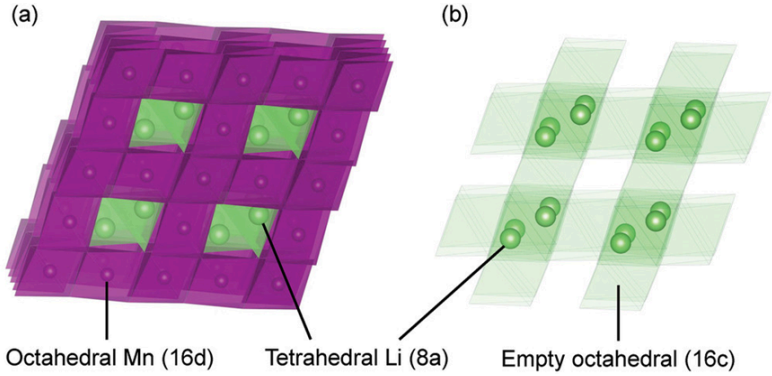

Figure 2. (a) Crystal structure and (b) ion transport pathways of $LiMn_2O_4$

During charging, $LiMn_2O_4$ undergoes the oxidation reaction of $Mn^{3\cdot5+}$→Mn^{4+} at 4.0 V, while Li^+ gradually deintercalates from the 8a site, leaving only the $[Mn_2]16dO_4$ skeleton. This process is structurally reversible. During discharging, with the reduction reaction of Mn^{4+}→$Mn^{3\cdot5+}$, Li^+ re-intercalates into the 8a site, restoring the previous $LiMn_2O_4$ structure. However, due to the large number of cation vacancies in $LiMn_2O_4$, further Li^+ intercalation can be achieved. During further discharging, a plateau appears at 3 V, corresponding to the reduction reaction of $Mn^{3\cdot5+}$→Mn^{3+}, accompanied by the transformation of $LiMn_2O_4$→$Li_2Mn_2O_4$ and the transfer of Li^+ from the 8a site to the 16c site for storage. Mn^{3+} has a high-spin $t_2g^3eg^1$ electron configuration in an octahedral field environment, and the uneven electron distribution in the two eg orbitals leads to the Jahn-Teller effect, resulting in strong lattice distortion. Therefore, a phase transition from cubic spinel phase to tetragonal spinel phase occurs in the low-voltage region, and the huge lattice expansion causes severe structural damage and rapid capacity fading. Meanwhile, Mn^{3+} on the surface undergoes a disproportionation reaction to generate Mn^{2+} and Mn^{4+}, and the generated Mn^{2+} is soluble, leading to irreversible Mn dissolution loss.Therefore, the current spinel $LiMn_2O_4$ can only be used in the voltage range above 3 V, with a theoretical specific capacity of 148 mAh g^{-1} at the 4 V working voltage plateau, and the mass energy density it can provide is close to that of $LiFePO_4$. However, in the high-voltage range, $LiMn_2O_4$ undergoes Mn dissolution during cycling, leading to capacity fading, and even high-temperature service environment will exacerbate Mn dissolution. Mn dissolution can be attributed to the inevitable generation of Mn^{3+} during the cycling of $LiMn_2O_4$ and the subsequent Jahn-Teller effect and disproportionation reaction. To solve this problem, on the one hand, researchers have effectively isolated $LiMn_2O_4$ from electrolyte contact and inhibited the disproportionation reaction of Mn^{3+} through surface coating layers (e.g., Al_2O_3, ZrO_2, Li_2ZrO_3, AlF_3 and $Li_3V_2(PO_4)_3$, etc.). On the other hand, low-valent cationic elements (e.g., Li^+, Mg^{2+}, Zn^{2+}, Co^{2+}, Ni^{3+}, Al^{3+}, etc.) are introduced to increase the average valence state of Mn, thereby suppressing the Jahn-Teller effect.

Among them, spinel $LiNi_{0.5}Mn_{1.5}O_4$ can be obtained by introducing low-valent Ni^{2+} to replace 1/4 of Mn elements. The Mn element in the crystal will remain +4 valence during charge-discharge, which significantly inhibits the Jahn-Teller effect and improves structural stability. Although $LiNi_{0.5}Mn_{1.5}O_4$ only has a theoretical specific capacity of 147 mAh g^{-1}, the redox reactions of Ni^{2+}/Ni^{3+} and Ni^{3+}/Ni^{4+} occur during cycling, resulting in a charge-discharge plateau as high as 4.7 V. Therefore, the theoretical energy density of this material is increased from 500 Wh kg^{-1} of $LiMn_2O_4$ to 700 Wh kg^{-1}, making it a more commercially attractive spinel-phase cathode material. Based on

DOI: 10.54254/2755-2721/2026.AD33327

the occupancy of Ni^{2+} and Mn^{4+}, $LiNi_{0.5}Mn_{1.5}O_4$ can be divided into two different cubic spinel structures: Ni/Mn disordered Fd-3m space group and Ni/Mn ordered $P4_332$ space group. When the calcination temperature of the material is lower than 700 ℃, ordered $LiNi_{0.5}Mn_{1.5}O_4$ is formed. In the unit cell, the 16d site splits into 4a and 12b sites, occupied by Ni^{2+} and Mn^{4+} respectively. The octahedral 16c vacancy splits into octahedral 4a and octahedral 12d vacancies, forming new Li^+ diffusion paths: 8c→4a→8c and 8c→12d→8c. The diffusion difficulty of the latter is greater than that of the 8a→16c→8a path of disordered $LiNi_{0.5}Mn_{1.5}O_4$, and it accounts for 75% of the diffusion path. Therefore, ordered $LiNi_{0.5}Mn_{1.5}O_4$ is not conducive to Li^+ intercalation/deintercalation, and the Li^+ diffusion coefficient is 1-2 orders of magnitude lower than that of the disordered phase. When the calcination temperature is higher than 700 ℃, Ni^{2+} randomly replaces Mn^{4+}, forming disordered $LiNi_{0.5}Mn_{1.5}O_4$. Meanwhile, oxygen loss occurs under high-temperature conditions, resulting in a certain amount of Mn^{3+} remaining in the material. Due to the presence of Mn^{3+}, disordered $LiNi_{0.5}Mn_{1.5}O_4$ exhibits an electronic conductivity 2.5 orders of magnitude higher than that of the ordered structure, thus showing more excellent rate performance. However, high-voltage electrolytes matching the working voltage plateau of $LiNi_{0.5}Mn_{1.5}O_4$ have not been successfully developed, limiting the large-scale application of the material.

4. Layered cathode materials

Layered transition metal oxide $LiCoO_2$ was first reported for its electrochemical activity by Goodenough's research group in 1980, and was commercialized by Sony Corporation of Japan in 1991 with carbon material anodes, and is currently widely used in the 3C electronic product market. $LiCoO_2$ belongs to the hexagonal system with a typical α-$NaFeO_2$ structure, belonging to the R-3m space group, with unit cell parameters a=2.816(2) Å and c=14.08(1) Å. In the unit cell, O occupies the 6c site and forms a face-centered cubic close-packed framework. Li^+ and Co^{3+} occupy the 3a and 3b sites respectively, forming LiO_6 octahedra and CoO_6 octahedra with O atoms respectively. As shown in Figure 3, along the c-axis direction, O atoms are stacked in the ABCABC sequence, and Li^+ and Co^{3+} are alternately arranged to form Li layers and CoO_2 layers. This layered structure is usually named O3 phase ("O" corresponds to Octahedron, representing Li^+ occupying the center of the octahedron, and "3" corresponds to the number of CoO_2 layers in a single unit cell). During the charge-discharge process of the battery, Li^+ migrates between CoO_2 layers in a two-dimensional manner, with a diffusion coefficient of about 10^{-9} cm^2 s^{-1}, between that of $LiFePO_4$ with one-dimensional channels and spinel $LiMn_2O_4$ with three-dimensional migration channels.

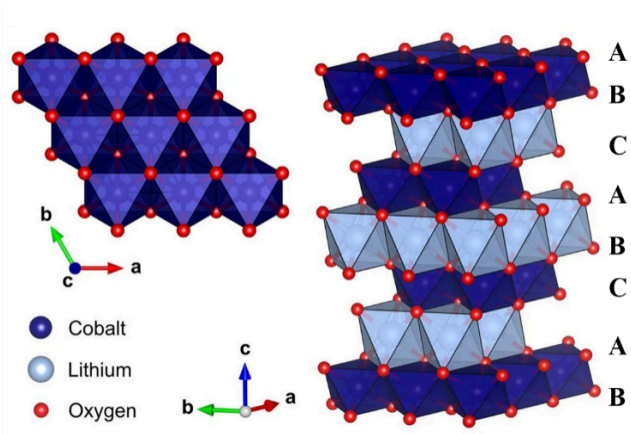

Figure 3. Schematic diagram of the crystal structure of $LiCoO_2$

DOI: 10.54254/2755-2721/2026.AD33327

$LiCoO_2$ has a high theoretical specific capacity of 274 mAh g^{-1}. However, unlike $LiFePO_4$ and $LiMn_2O_4$ whose structural frameworks are not affected by Li^+ intercalation/deintercalation, since the Li layer is also part of the $LiCoO_2$ structural framework, a large amount of Li^+ deintercalation during high-voltage charging will lead to structural collapse, and then cause continuous deterioration of electrochemical performance. The structural evolution of Li_xCoO_2 during delithiation can be divided into two stages: $0.45 \leq x \leq 1$ and $0 \leq x < 0.45$. Firstly, at x=0.93-0.75, Li_xCoO_2 transforms from O3 (I) phase to O3 (II) phase. During this phase transition, with the decrease of Li^+ content, the electronic property of the material changes from semiconductor to metallic property, and the electronic conductivity increases. Then, near x=0.5, the crystal undergoes two phase transitions: hexagonal→monoclinic→hexagonal. When $x < 0.45$, with the deintercalation of Li^+, the crystal further undergoes phase transitions from O3 to H1-3 and even O1 phase (H1-3 is a mixture of O3 phase and O1 phase), leading to severe shrinkage of the unit cell along the c-axis and structural collapse. In addition, at high voltage, $LiCoO_2$ undergoes lattice oxygen oxidation and loss, and spinel Co_3O_4 is irreversibly generated on the surface to hinder Li^+ transport. In recent years, a large number of studies have focused on bulk doping and interface optimization, and the phase structure stability of $LiCoO_2$ during charge-discharge has been gradually improved. Over the past 30 years, the application voltage of commercial $LiCoO_2$ has been increased from 4.2 V to 4.45 V, and the actual specific capacity has also been increased from about 140 mAh g^{-1} to 170-175 mAh g^{-1}. At present, by combining bulk and interface optimization strategies, the cut-off voltage of $LiCoO_2$ can be increased to 4.6 V (vs Li/Li^+), thereby increasing the specific capacity and mass energy density to 220 mAh g^{-1} and 885.9 Wh kg^{-1} respectively.

5. Conclusion

This paper systematically reviews the development history and latest research progress of cathode materials for lithium-ion batteries, focusing on the crystal structure, electrochemical characteristics and challenges of three typical cathode materials: olivine structure, spinel structure and layered oxides. Olivine-structured materials (e.g., $LiFePO_4$) have excellent cycle stability and safety, but low intrinsic electronic/ionic conductivity, requiring carbon coating, nanocrystallization or ion doping to improve rate performance. Although its derivative $LiFe_xMn_{1-x}PO_4$ can increase energy density, it still needs to solve the problem of Jahn-Teller effect caused by Mn^{3+}. Spinel-structured materials (e.g., $LiMn_2O_4$) have three-dimensional lithium ion diffusion channels and good rate performance, but the Jahn-Teller effect and disproportionation reaction of Mn^{3+} lead to capacity fading. Element substitution (e.g., Ni doping to prepare $LiNi_{0.5}Mn_{1.5}O_4$) and surface coating can effectively suppress structural degradation and improve high-voltage stability.

References

[1] Yi T-F, Mei J, Zhu Y-R. Key strategies for enhancing the cycling stability and rate capacity of $LiNi_{0.5}Mn_{1.5}O_4$ as high-voltage cathode materials for high power lithium-ion batteries. Journal of Power Sources, 2016, 316: 85-105.

[2] Wang H, Tan T A, Yang P, et al. High-rate performances of the Ru-doped spinel $LiNi_{0.5}Mn_{1.5}O_4$: Effects of doping and particle size. The Journal of Physical Chemistry C, 2011, 115(13): 6102-6110.

[3] Wang L, Li H, Huang X, et al. A comparative study of Fd-3m and $P4_332$ "$LiNi_{0.5}Mn_{1.5}O_4$". Solid State Ionics, 2011, 193(1): 32-38.

[4] Yang M-C. Strategies to improve the electrochemical performance of electrodes for lithium-ion batteries [D]. Florida, USA: University of Florida, 2012.

[5] Merryweather A J, Schnedermann C, Jacquet Q, et al. Operando optical tracking of single-particle ion dynamics in batteries. Nature, 2021, 594: 522-526.